Physics Letters A 375 (2011) 2071–2074

Contents lists available at ScienceDirect

Physics Letters A

www.elsevier.com/locate/pla

Thickness and in-plane elasticity of graphane

F. Scarpa [a,*], R. Chowdhury [b], S. Adhikari [b]

[a] Advanced Composites Centre for Innovation and Science, University of Bristol, BS8 1TR Bristol, UK
[b] Multidisciplinary Nanotechnology Centre, Swansea University, SA2 8PP Swansea, UK

ARTICLE INFO

Article history:
Received 7 December 2010
Received in revised form 14 March 2011
Accepted 27 March 2011
Available online 2 April 2011
Communicated by R. Wu

Keywords:
Hydrogenated graphene
Thickness
Mechanical properties

ABSTRACT

The thickness and in-plane mechanical properties (Young's, shear modulus, Poisson's ratios) of fully hydrogenated graphene (graphane) sheets are predicted using a molecular mechanics approach. The equilibrium lengths and bond angles distortions used for the graphane models are obtained from Density Functional Theory (DFT) simulations. Our models compare well with existing data on the uniaxial properties of graphane and graphene sheets from first principle and Molecular Dynamics (MD) simulations, highlight a special orthotropic mechanical behaviour for graphane, and identify thickness and shear stiffness values which are peculiar of hydrogenated graphene.

1. Introduction

Hydrogenated graphene has been considered as one of the possible purveyors of the next generation materials for hydrogen storage and two-dimensional electronics [1–4], as well as opening new possibilities in transport-based nanosensors similarly to graphene [5,6]. The gap opened by the adsorption of graphene allows the graphene to undergo a transition from metallic state to insulator, and creates either a chair or boat structure, depending whether the hydrogen groups are uniformly or alternately dispersed on the two sides of the graphene sheet (Fig. 1a) [7,1,8]. The in-plane structural distorsions induced by the presence of the hydrogenated groups lead to a lattice with internal angles and equilibrium length different from the 120° and 1.42 Å of the sp^2 pristine configuration [9], similarly to what has been observed also in boron nitride sheets [10]. The use of XPS [11] and TEM techniques [12] has revealed that the energy required for breaking a bond between 2-coordinate atoms is 1.32 time the one needed to break a C–C bond between 3-coordinated atoms. The presence of tilt grain boundaries providing 5- and 7-membered ring could enhance also the strength of GNR substantially [13]. However, although extensive studies have been also performed recently to discern the transport and electronics properties of graphane [3,14,15], only a limited amount of work has been dedicated to understand the implications that the adsorption of graphene has on the mechanical properties of this nanostructure [16,17].

In this work we identify for the first time three novel aspects related to the hydrogenation of graphene. The first is the in-plane orthotropic nature of the graphane elasticity. In [16] and [17], the in-plane mechanical properties of 100% hydrogenated graphene are assumed to be isotropic. With our approach, we will show that an effective way to interpret the uniaxial in-plane mechanical properties of graphane is to consider the nanomaterial as *special orthotropic* – i.e., with a spatial dependence of its mechanical behaviour. While for pristine graphene in finite sizes the anisotropy is given by the edges [18–20], in graphane the presence of the hydrogenation contributes also to this less usual (although not uncommon) mechanical characteristic. The second novel aspect of this work is the identification of the in-plane shear stiffness for 100% hydrogenated graphene, a mechanical parameter which has not been evaluated for this particular nanostructure, to the best of our knowledge. The third novelty contained in this work is the identification of the equivalent thickness for *graphane*, using an approach developed and validated on carbon nanotubes and graphene. The knowledge of the thickness is instrumental to identify equivalent Young's modulus and other mechanical properties for the use and assessment of hydrogenated graphene for nanosensors and/or nanocomposite applications.

2. Modelling

In this work, the determination of the in-plane mechanical properties of 100% hydrogenated graphene is performed using an atomistic–finite element approach (Fig. 1) that the authors have developed to simulate the mechanics of pristine graphene [21,22], carbon nanotubes [23,24] and heterojunctions [25]. To compute the equivalent stiffness for the C–C bond in the C–OH group, we consider the equality between the steric harmonic potential and the mechanical strain energies of a deep shear beam [21]:

* Corresponding author.
E-mail address: f.scarpa@bristol.ac.uk (F. Scarpa).

0375-9601/$ – see front matter
doi:10.1016/j.physleta.2011.03.050

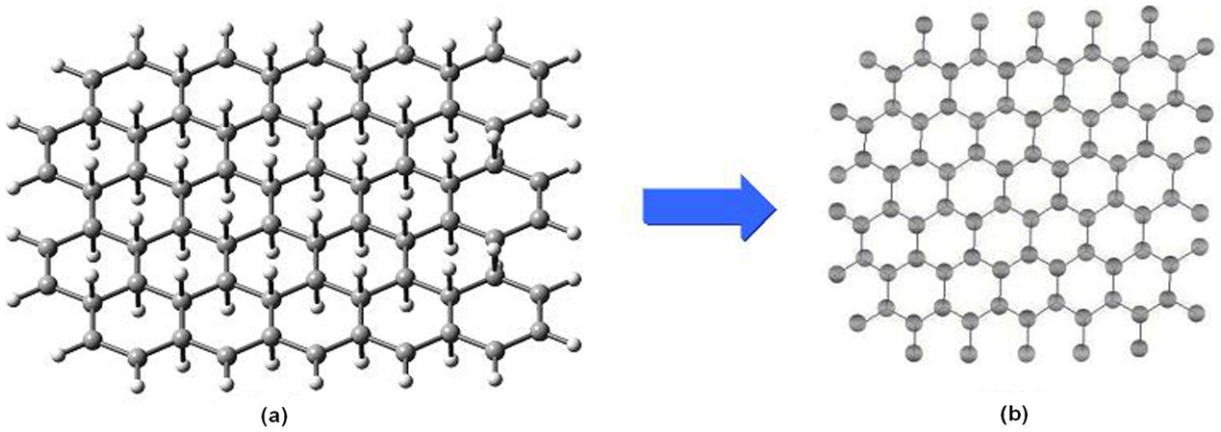

Fig. 1. (a) Molecular representation of a (5, 5) 100% hydrogenated graphene with boat-like configuration; (b) 2D atomistic–FE configuration of the in-plane C–C bonds as a projection of the 3D graphane sheet in (a).

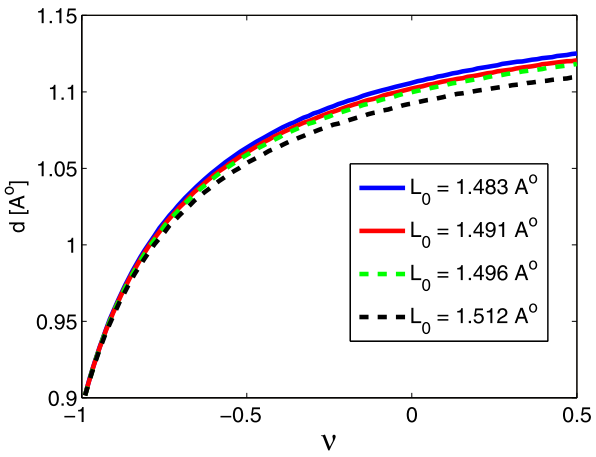

Fig. 2. Dependence of C–C bond thickness versus the equivalent Poisson's ratio ν for the various equilibrium configurations in [29].

$$\frac{k_r}{2}(\delta r)^2 = \frac{EA}{2L}(\delta r)^2$$
$$\frac{k_\tau}{2}(\delta\varphi)^2 = \frac{GJ}{2L}(\delta\varphi)^2$$
$$\frac{k_\theta}{2}(\delta\theta)^2 = \frac{EI}{2L}\frac{4+\Phi}{1+\Phi}(\delta\theta)^2 \tag{1}$$

where δr, $\delta\varphi$ and $\delta\theta$ are the infinitesimal axial, out-of-plane and in-plane rotations of the bond respectively. The deformation of a deep shear beam is affected by the shear resistance distributed over the cross-section by the following shear factor [26,27]:

$$\Phi = \frac{12EI}{GA_sL^2} \tag{2}$$

In (2), $A_s = A/F_s$ is the reduced cross-section of the beam by the shear correction term F_s [26]:

$$F_s = \frac{6+12\nu+6\nu^2}{7+12\nu+4\nu^2} \tag{3}$$

The insertion of (2) and (3) in (1) leads to an nonlinear relation between the thickness d and the Poisson's ratio ν of the equivalent beam [21]:

$$k_\theta = \frac{k_r d^2}{16}\frac{4A+B}{A+B} \tag{4}$$

where:

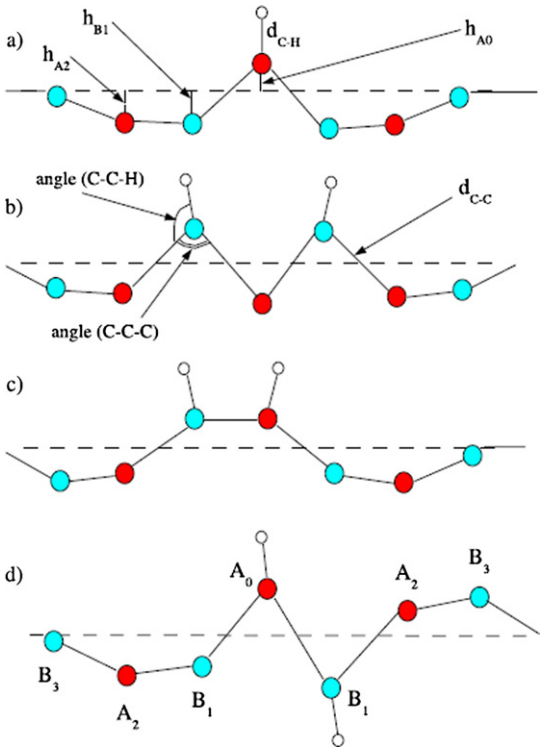

Fig. 3. Local distorsion of graphene at chemisorption of (a) single hydrogen atom (A_0), (b) two hydrogen atoms bonded with carbon atoms from the same sublattice (A_0–A_2), (c) hydrogen atoms bonded with carbon atoms from the same side of graphene (A_0–B_1) and (d) two hydrogen atoms bonded with neighbouring carbon atoms from both sides of the graphene layer (A_0–B_1p). (From [29].)

$$A = 112L^2k_\tau + 192L^2k_\tau\nu + 64L^2k_\tau\nu^2 \tag{5}$$

$$B = 9k_rd^2 + 18k_rd^4\nu + 9k_rd^4\nu^2 \tag{6}$$

The values for the force constants are derived from the Universal Force Field (UFF) model ($k_r = 4.39\times10^{-7}$ N mm^{-1}, $k_\theta = 8.76\times10^{-10}$ N nm rad^{-2}, $k_\tau = 2.78\times10^{-10}$ N nm^{-1} rad^{-2} [28]). The equivalent mechanical properties of the C–C bond (see Fig. 2) can be determined performing a nonlinear optimisation of (1) using a Marquardt algorithm. The values of the equilibrium lengths L in Eqs. (5) and (6) are 1.483 Å, 1.491 Å, 1.496 Å and 1.512 Å, corresponding to the four bond lengths obtained in [29] using DFT calculations (see Fig. 3 for the equilibrium structures of the distorted graphene due to chemisorption). The curves can be represented with good accuracy ($R^2 = 0.99$ with 95% confidence)

Table 1
Uniaxial tensile properties for the graphane configurations loaded along the zig-zag (x) direction.

Bond type	Angle C–C	L [Å]	d [Å]	E_x [TeV/Å^3]	ν_{xy}	Y_x [TeV/Å^2]
A_0–B_1p	106.7°	1.436	1.129	9.940	0.392	11.222
A_0	115.4°	1.422	1.139	12.129	0.458	13.185
A_0–A_2	116.6°	1.437	1.139	9.786	0.394	11.146
A_0–B_1	117.5°	1.454	1.130	13.916	0.517	15.725

Table 2
Uniaxial tensile properties for the graphane configurations loaded along the armchair (y) direction.

Bond type	Angle C–C	L [Å]	d [Å]	E_y [TeV/Å^3]	ν_{yx}	Y_y [TeV/Å^2]
A_0–B_1p	106.7°	1.437	1.139	16.265	0.675	18.526
A_0	115.4°	1.459	1.137	14.213	0.547	16.016
A_0–A_2	116.6°	1.446	1.130	14.147	0.527	15.986
A_0–B_1	117.5°	1.454	1.130	13.916	0.517	15.725

Table 3
Uniaxial tensile properties for the graphane configurations loaded in simple shear.

Bond type	Angle C–C	L [Å]	d [Å]	G_{xy} [TeV/Å^3]	Y_{xy} [TeV/Å^2]
A_0–B_1p	106.7°	1.474	1.140	4.941	5.633
A_0	115.4°	1.459	1.142	4.698	5.365
A_0–A_2	116.6°	1.446	1.145	4.665	5.341
A_0–B_1	117.5°	1.454	1.145	4.621	5.291

with an exponential fit of the type $d = a_1 e^{a_2 \nu} + a_3 e^{a_4 \nu}$. For the case of $L_0 = 1.512$ Å, the coefficients are $a_1 = 1.099$, $a_2 = 0.0210$, $a_3 = -0.00639$, $a_4 = -3.296$ (Fig. 2).

We simulate the in-plane graphane properties representing the graphene sheet as a truss assembly of equivalent structural beams (the C–C bonds) with parametric thickness d and equivalent ν (Fig. 1) [21]. The uniaxial properties (Young's moduli E_x and E_y) are predicted loading the lattice sheets at one end along the x and y directions (zig-zag and armchair respectively) with imposed strains $\epsilon_{x,y}$ of 0.05%, while the opposite side is constrained through a clamp condition. For the in-plane shear modulus G_{xy}, a uniform shear strain is applied at the boundaries of the graphene sheet. The Poisson's ratios have been calculated from the ratio between the homogenised lateral strain to the imposed tensile strain with the minus sign [21,30]. The average equilibrium lengths and angles of the structural truss assemblies are derived from the structural configurations identified by Boukhvalov et al. [29]. The mechanical loading simulations have been carried on graphane sheets with 6440 in-plane C–C bonds, and sheet aspect ratio equal to 1.1. The rationale behind the use of such large graphane sheets models was to apply the mechanical homogenisation process over a large number of lattice units, and obtain stiffness properties tending asymptotically to an equivalent homogeneous medium [31]. Prior to the determination of the equivalent mechanical properties of the graphane sheets, the total potential energy of the graphane systems is minimised versus the thickness d during the static loading using a two-steps zero-order and first-order optimisation scheme [21,22]. When the minimised configurations are identified, the Young's moduli are calculated as $E_i = \sigma_i/\epsilon_i$, where σ_i are the stresses along the i-direction obtained averaging the reaction forces over the loaded ends of the sheets. The shear modulus G_{xy} is extracted from the second derivative of the strain energy versus the shear strain [21].

3. Results

Tables 1–3 show the thickness, moduli (Young's and shear), Poisson's ratios and rigidities (product between modulus and thickness) for the four structural configurations from Boukhvalov and co-workers. The thickness values identified through the minimisation of the potential energy range between 1.129 and 1.145 Å and seems also dependent on the loading conditions for the different types of bond structures (see Tables 1, 2 and 3, fourth columns). The values of the graphane thickness compare with the 1.317 Å from Hemmasizadeh et al. [32], the 1.0 Å from Scarpa et al. [22] observed during bending of pristine graphene, and the 1.0 Å calculated by Sears and Batra in carbon nanotube structures [33]. Similar values have been also identified for C–C sp^2 in single wall carbon nanotubes. The theoretical reproduction of the elastic modulus and melting point in [34] has derived the effective thickness of single-walled CNT as 1.42 Å, with the C–C bond having an equilibrium length of 1.25 Å, with an elastic modulus of 2.6 TPa. These values are different from the 3.4 Å (the graphitic interlayer atomic distance) assumed by Pei et al. [16] for graphane sheets. Moreover, the thickness of pristine graphene layers under in-plane loading appears to be lower than the one of graphane sheets (see the 0.57 Å of Huang et al. [35], 0.8 Å of Gupta and Batra [36], and 0.74 Å of Scarpa and co-workers [21]). The identified graphane thickness values involve an equivalent Poisson's ratio ν for the C–C bond material around 0.44–0.46, suggesting that the bonds do mechanically behave like hyperelastic materials [37]. For all the bond types, the special orthotropic condition ($E_x \nu_{yx} = E_y \nu_{xy}$ [30]) is satisfied with small discrepancies between 4 and 6%, due to the edge effects and finite size of the sheets, similarly to what has been observed in single graphene layers [20,21]. For special orthotropic sheets, it is possible to use the geometric mean $Y_g = \sqrt{Y_x Y_y}$ and $\nu_g = \sqrt{\nu_{xy}\nu_{yx}}$ to identify a stiffness and Poisson's ratio constant for the material [22]. For the different bond types (A_0–B_1p, A_0, A_0–A_2, A_0–B_1), we have values of Y_g equal to 231, 214, 240 and 252 N m^{-1} respectively, which compares well with the 243 N m^{-1} identified by Topsakal et al. using first principles plane wave calculations [17]. Pei and co-workers predict in-plane tensile rigidities between 200 and 207 N m^{-1} from MD simulations on 100% hydrogenated graphene based on the AIREBO potential [16]. Our model also predicts an equivalent tensile rigidity for pristine single layer graphene sheets of 330 N m^{-1} [21,22], which again compares well with the 335 N m^{-1} in [17], and the experimental 340 N m^{-1} obtained from AFM bending tests [38]. The effect of the hydrogena-

tion leads to a general decrease of the in-plane stiffness between 24% for A_0–B_1 bond type, to the 35% of A_0 one, with the A_0–A_2 bond featuring a stiffness drop of 27%. The in-plane stiffness decrease is in line with the 27% observed by Topsakal and co-workers [17], and 28% calculated by Pei et al. [16]. The geometric mean of the Poisson's ratios ν_g derived from Tables 1–2 vary between 0.45 for the A_0 bond type to 0.52 for the A_0–B_1. Those values are notably higher than the 0.07 identified in [17]. For finite size pristine graphene sheets (and taking into account a special orthotropic mechanical behaviour), our model predicts an in-plane $\nu_g = 0.51$. However, we note that Reddy et al. determine a $\nu_g = 0.47$ for finite size graphene layers using a first generation Tersoff–Brenner potential with Cauchy–Borne rule in similar sized sheets [19]. In lattice structures with in-plane bond angles different from 120° undergoing stretching–hinging deformations of the bonds, it is expected to have equivalent Poisson's ratios with different ν_{xy} and ν_{yx} values, to satisfy the special orthotropicity relation [39]. Our simulations for the fully hydrogenated graphene shows that the A_0–B_1p bond structure provides the highest difference in terms of Poisson's ratios ($\nu_{xy} = 0.392, \nu_{yx} = 0.675$), with a orthotropicity ratio $Y_x/Y_y = 0.6$, well below the 0.82 identified in pristine graphene [21,19]. The higher difference between Young's moduli in graphane along the two principal directions (armchair and zigzag) has to be ascribed not only to edges effects like in graphene, but also to the angular distortion produced by the chemisorption of the hydrogen atoms. The shear modulus G_{xy} (Table 3) has an average around 4.7 TeV Å^{-3} for the different bond types. For pristine graphene sheets, our model predicts a shear rigidity Y_{xy} equal to 10.48 TeV Å^{-3} [21], in line with the experimental 9.17 TeV Å^{-3} observed in graphitic layers [40]. The graphane sheets appear to have a significant lower in-plane shear rigidity compared to graphene layers, with an average drop of 55%, a decrease comparatively higher than the one observed for the uniaxial tensile properties. This fact could be explained considering both the lower stretching force constant k_r used compared the value used in single layer graphene (AMBER and Morse potential [21]), and the higher thickness value of the graphene compared to pristine graphene when loaded in the (x, y) plane. A high thickness value leads to greater deformations of the equivalent structural deep shear beams used to represent the C–C bonds, providing an overall higher compliance of the graphane structure when subjected to global shear loading. It is worth noticing that the shear rigidities for the graphane configurations appear to follow the relation $Y_{xy} \approx Y_g/2/(1+\nu_g)$, with discrepancies ranging between 4% and 8%.

4. Conclusions

The fully hydrogenated graphene (graphane) shows typical in-plane special orthotropic mechanical properties, with high values of anisotropic ratio (in particular for the A_0–B_1p structure). For the different loading cases examined, the thickness is above 1.1 Å. The in-plane uniaxial stiffness is reduced between 24% and 35% compared to the pristine graphene layer, with a more significant decrease for the in-plane shear rigidity, always compared to the non-hydrogenated graphene case.

References

[1] D.K. Samarakoon, X.-Q. Wang, ACS Nano 3 (12) (2009) 4017, doi:10.1021/nn901317d, http://pubs.acs.org/doi/pdf/10.1021/nn901317d, pMID: 19947580.
[2] J.O. Sofo, A.S. Chaudary, G.D. Barber, Phys. Rev. B 75 (2007) 153401.
[3] J. Jones, K. Mahajan, W. Williams, P. Ecton, Y. Mo, J. Perez, Carbon 48 (8) (2010) 2335, doi:10.1016/j.carbon.2010.03.010.
[4] Y. Wang, S. Shi, Solid State Commun. 150 (31–32) (2010) 1473, doi:10.1016/j.ssc.2010.05.031.
[5] Y. Zhang, Y. Tan, H. Stormer, P. Kim, Nature 438 (7065) (2005) 201, doi:10.1038/nature04235.
[6] R. Chowdhury, S. Adhikari, P. Rees, S.P. Wilks, F. Scarpa, Phys. Rev. B 83 (4) (2011) 045401, doi:10.1103/PhysRevB.83.045401.
[7] D.C. Elias, R.R. Nair, T.M.G. Mohiuddin, S.V. Morozov, P. Blake, M.P. Halsall, A.C. Ferrari, D.W. Boukhvalov, M.I. Katsnelson, A.K. Geim, K.S. Novoselov, Science 323 (2009) 610.
[8] M.Z.S. Flores, P.A.S. Autreto, S.B. Legoas, D.S. Galvao, Nanotechnology 20 (2009) 465704, doi:10.1088/0957-4484/20/46/465704.
[9] A.K. Geim, K.S. Novoselov, Nature Mater. 6 (3) (2007) 183.
[10] Y. Wang, Phys. Status Solidi Rapid Res. Lett. 4 (2010) 34.
[11] C.Q. Sun, Y. Sun, Y.G. Nie, Y. Wang, J.S. Pan, G. Ouyang, L.K. Pan, Z. Sun, J. Phys. Chem. C 113 (37) (2009) 16464, doi:10.1021/jp905336j.
[12] C.O. Girit, J.C. Meyer, R. Erni, M.D. Rossell, C. Kisielowski, L. Yang, C.H. Park, M.F. Crommie, M.L. Cohen, S.G. Louie, A. Zettl, Science 232 (2009) 1705.
[13] R. Grantab, V.B. Shenoy, R.S. Ruoff, Science 330 (6006) (2010) 946, doi:10.1126/science.1196893, http://www.sciencemag.org/content/330/6006/946.full.pdf.
[14] H. Şahin, C. Ataca, S. Ciraci, Phys. Rev. B 81 (20) (2010) 205417, doi:10.1103/PhysRevB.81.205417.
[15] G. Savini, A.C. Ferrari, F. Giustino, Phys. Rev. Lett. 105 (3) (2010) 037002, doi:10.1103/PhysRevLett.105.037002.
[16] Q. Pei, Y. Zhang, V. Shenoy, Carbon 48 (3) (2010) 898, doi:10.1016/j.carbon.2009.11.014.
[17] M. Topsakal, S. Cahangirov, S. Ciraci, Appl. Phys. Lett. 96 (9) (2010) 091912, doi:10.1063/1.3353968.
[18] C.D. Reddy, S. Rajendran, K.M. Liew, Int. J. Nanosci. 4 (4) (2005) 631.
[19] C.D. Reddy, S. Rajendran, K.M. Liew, Nanotechnology 17 (2006) 864.
[20] C.D. Reddy, A. Ramasubramaniam, V.B. Shenoy, Y.W. Zhang, Appl. Phys. Lett. 94 (10) (2009) 101904.
[21] F. Scarpa, S. Adhikari, A.S. Phani, Nanotechnology 20 (2009) 065709.
[22] F. Scarpa, S. Adhikari, A.J. Gil, C.D.L. Remillat, Nanotechnology 21 (2010) 125702, doi:10.1088/0957-4484/21/12/125702.
[23] F. Scarpa, S. Adhikari, J. Phys. D: Appl. Phys. 41 (2008) 085306, doi:10.1088/0022-3727/41/8/085306.
[24] F. Scarpa, L. Boldrin, H.X. Peng, C.D.L. Remillat, S. Adhikari, Appl. Phys. Lett. 97 (2010) 151903, doi:10.1063/1.3499748, (3 pp).
[25] F. Scarpa, J.W. Narojczyk, K.W. Wojciechowski, Phys. Status Solidi B 248 (1) (2011) 82, doi:10.1002/pssb.201083984.
[26] T. Kaneko, J. Phys. D: Appl. Phys. 8 (1974) 1927.
[27] J.S. Przemienicki, Theory of Matrix Structural Analysis, McGraw–Hill, New York, 1968.
[28] A.K. Rappe, C.J. Casewit, K.S. Colwell, W.A. Goddard, W.M. Skiff, J. Amer. Chem. Soc. 114 (25) (1992) 10024, doi:10.1021/ja00051a040.
[29] D.W. Boukhvalov, M.I. Katsnelson, A.I. Lichtenstein, Phys. Rev. B 77 (2008) 035427.
[30] Y. Fung, Foundations of Solid Mechanics, Prentice Hall, 1968.
[31] D. Caillerie, A. Mourat, A. Raoult, J. Elasticity 84 (2006) 33.
[32] A. Hemmasizadeh, M. Mahzoon, E. Hadi, Thin Solids Films 416 (2008) 7636.
[33] A. Sears, R.C. Batra, Phys. Rev. B 69 (23) (2004) 235406.
[34] C.Q. Sun, H.L. Bai, B.K. Tai, S. Li, E.Y. Jiang, J. Phys. Chem. B 107 (2003) 7544.
[35] Y. Huang, J. Wu, K.C. Hwang, Phys. Rev. B 74 (2006) 245413.
[36] S.S. Gupta, R.C. Batra, J. Comput. Theor. Nanosci. 7 (2010) 2151.
[37] K. Suzuki, S. Nomura, J. Composite Mater. 41 (9) (2007) 1123.
[38] C. Lee, X. Wei, J.W. Kysar, J. Hone, Science 321 (5887) (2008) 385.
[39] I.G. Masters, K.E. Evans, Composite Struct. 35 (4) (1996) 403.
[40] O.L. Blakslee, et al., J. Appl. Phys. 44 (8) (1970) 3373.